

MASS DISTRIBUTION AND BULGE FORMATION IN THE MILKY WAY GALAXY

Ortwin Gerhard¹

Abstract. In its first part, this paper summarizes recent work on the mass and shape of the Galactic dark halo. The second part presents a review of the large-scale structure of the Milky Way, and of the evidence that the inner Galaxy is dominated by baryonic matter. This is briefly compared with the predictions of Λ CDM and MOND. Finally, a summary is given of bulge formation from clumpy, gas-rich disks, a process which may give rise to old, disk-like, α -rich bulges similar to the Galactic bulge.

1 Introduction

Our position inside the Milky Way has both advantages and drawbacks. On the one hand, a number of experiments are possible that give complementary information on Galactic structure to that attainable for external galaxies. Notable examples are microlensing surveys, three-dimensional velocity data, local dynamical and stellar population measurements, determination of line-of-sight density distributions, etc. On the other hand, our view from inside the disk is often obscured, distance measurements are often needed but difficult, and deciphering the large-scale structure of the Galaxy is a much more involved process than from the image of an external galaxy. Both aspects are evident in the following sections: in §2, we review recent work on measuring the radial mass distribution and shape of the Galactic dark matter halo. Then in §3, we summarize constraints on the distribution of baryonic matter in the Milky Way, based on NIR, gas kinematic, and microlensing data. Finally in §4, we discuss a model of bulge formation from clumpy gas-rich disks which has some promise for understanding Galactic bulge observations.

¹ Astronomisches Institut, Universität Basel, Venusstrasse 7, CH-4102 Binningen, Switzerland; current address: Max-Planck-Institut für Extraterrestrische Physik, Giessenbachstrasse, D-85748 Garching, Germany

2 The Galactic Dark Halo

2.1 Total Halo Mass and Radial Mass Distribution

HI radial velocity measurements constrain the Galactic rotation curve to radii $\lesssim 20$ kpc (Honma & Sofue 1997). Determinations of the total mass of the Galaxy are therefore based on the kinematics of globular clusters, satellite galaxies, and distant halo stars. There are not many of these; so further assumptions are needed. Based on radial velocities of 27 globular clusters and satellites at galactocentric $R > 20$ kpc, and additional proper motions for six of these, Wilkinson & Evans (1999) estimated the Milky Way's mass inside 50 kpc to be $M(50 \text{ kpc}) = 5.4_{-3.6}^{+0.2} \times 10^{11} M_{\odot}$, and its total mass as $M_t = 1.9_{-1.7}^{+3.6} \times 10^{12} M_{\odot}$. They used a Bayesian likelihood method, following earlier work by Little & Tremaine (1987) and Kochanek (1996), in which they assumed a spherical halo mass model with a truncation radius, and a particular ansatz for an anisotropic distribution function, assumed to describe the entire ensemble of tracers. Then the probability of the tracers to have their observed positions and velocities in this model is determined, and maximized over the model's total mass and constant anisotropy.

Sakamoto et al. (2003) applied this method to a larger sample of tracer objects, including 413 FHB halo stars, half of them with proper motions. Their estimate for $M_t = 2.5_{-1.0}^{+0.5} \times 10^{12} M_{\odot}$ is somewhat larger, while they obtain $M(50 \text{ kpc}) = 5.5_{-0.2}^{+0.0} \times 10^{11} M_{\odot}$, very similar to the earlier value but with much smaller errors. In my understanding this illustrates the limitations of this approach: the parametric model is seemingly very tightly constrained by the large number of new data points at mostly small radii; it is not flexible enough to adjust to these data locally while keeping the mass at large radii constrained by mostly the outer data points only. This suggests that these error bars should be viewed with caution.

Recently, Battaglia et al. (2005) have compiled a new halo tracer sample including distant halo giant stars with accurate distances and radial velocities. From this they determine more accurately the radial velocity dispersion profile (constant at $\sim 120 \text{ km s}^{-1}$ out to 30 kpc, then declining to $\sim 50 \text{ km s}^{-1}$ at 120 kpc). They then compare with dispersion profiles predicted from the Jeans equation for specified halo mass distribution and anisotropy. The data rule out an isothermal halo with constant anisotropy, but can be explained either by a dark matter halo truncated at large radii and constant velocity anisotropy, or by a NFW halo with less steep density profile whose velocity anisotropy becomes tangential at large radii. The total halo mass determined in these cases is $M_t = 1.2_{-0.5}^{+1.8} \times 10^{12} M_{\odot}$ and $M_v = 0.8_{-0.2}^{+1.2} \times 10^{12} M_{\odot}$, respectively. These values are smaller by a factor ~ 2 than the earlier total mass estimates, but are still consistent within the joint error ranges. For comparison, the favoured Λ CDM model from Klypin et al. (2002) has $M_v = 1.0 \times 10^{12} M_{\odot}$.

2.2 Halo Shape

Until recently, data constraining the shape of the Galactic halo were hard to come by. Olling & Merrifield (2000) found evidence for a near-spherical oblate halo with shortest-to-longest axis ratio $q_\rho = 0.8$, based on two techniques: (1) by comparing the mean halo density inferred from the rotation curve with the measured mass column density near the Sun, and (2) by comparing the predicted flaring of the gas disk in various flattened halo models with the measured flaring of the HI layer. However, these methods only agreed for somewhat small values of the Galactic constants R_0 and V_0 ; for more standard values, the second method would actually favour a prolate halo, in disagreement with the first.

The detailed mapping of the Sagittarius stream and the associated radial velocity measurements are bringing a significant advance to this subject. From the observation that the Carbon stars in the Sgr stream are consistent with a great circle on the sky, Ibata et al. (2001) argued that the precession rate must be slow and hence the halo nearly spherical. The recent all-sky map of the Sgr stream as traced by the M stars in the 2MASS survey (Majewski et al. 2003), together with other detections of the tidal streams of the Sgr galaxy (Martínez-Delgado et al. 2004), have provided strong constraints on the orbit of the tidal debris in the halo potential, and hence on the halo shape. From their simulations, Martínez-Delgado et al. (2004) obtain a halo potential flattening $q_\Phi = 0.85$. More recent fitting of the orbital planes (poles) of the Sgr leading and trailing debris in the 2MASS M giant data gives a very similar result (Johnston et al. 2005). However, Helmi (2004) finds that simulations of Sgr debris best agree with radial velocity measurements for part of the leading and trailing streams if the halo potential is prolate, with $q_\Phi = 1.25$. Radial velocities of course not only tell us about the speeding up of the stars as they fall towards the Galactic plane, which is different in oblate and prolate potentials. They also depend on how the orbit changes direction at the same time. It remains to be seen whether the positional and kinematic analyses of the Sgr stream can be reconciled for a triaxial halo potential, such as is indicated by SDSS starcounts for the *stellar* halo (Newberg & Yanny 2005).

3 Structure and Radial Mass Distribution of the Galaxy

3.1 Large-Scale Structure

The Milky Way is a barred galaxy with fairly weak outer spiral structure. Modern models of the luminosity distribution are based on NIR data, both from integrated light observations (COBE/DIRBE) and starcounts in the NIR. Bissantz & Gerhard (2002, hereafter BG) presented non-parametric models of the Galactic luminosity density interior to the Sun. Like several previous models (e.g., Binney, Gerhard & Spergel 1997) they are based on the COBE/DIRBE photometry, but also include a spiral arm model after Ortiz & Lépine (1993) and were verified a posteriori with the line-of-sight distributions of clump giant stars in several bulge fields (Stanek et al. 1997). The best models were obtained for bar angles $20 - 25^\circ$ relative to

the Sun-Galactic Centre line and had a thin bar (10:~3.5:3) with length ~ 3.5 kpc and a short disk scale-length, ~ 2.1 kpc. The latter is somewhat shorter than the disk scale-length obtained from DENIS (2.5 kpc, Robin et al. 2003) and 2MASS (~ 3 kpc, López-Corredoira et al. 2004) NIR starcounts. The 2MASS analysis also indicates that the disk profile flattens out inside ~ 4 kpc, rather than rising exponentially into the center. After subtracting the disk starcounts, inversion of the 2MASS counts results in a boxy bulge with slightly larger axis ratios than in the BG model (10:~5:4; López-Corredoira, Cabrera-Lavers & Gerhard 2005). Recently, Babusiaux & Gilmore (2005) obtained distance distributions of clump giant stars from deep NIR data in several bulge fields, which are consistent with a triaxial bar with in-plane axis ratio 10:3-4, bar angle $22 \pm 5.5^\circ$, extending to ~ 2.5 kpc, and circumscribed by an inner ring. Thus a fairly consistent picture of the inner Galaxy has emerged, with perhaps the main uncertainty being the density distribution of the disk inside a few kpc.

Taking the BG model with constant NIR mass-to-light ratio as a mass model, Bissantz, Englmaier & Gerhard (2003) simulated the Galactic gas flow in the Galactic gravitational potential. Comparing simulated (l, v) -plots with the observed CO (l, v) -diagram they determined the pattern speeds of the Galactic bar and spiral arms. The observed (l, v) -plot is best reproduced if the bar corotation radius is ~ 3.5 kpc, consistent with Dehnen's (2000) independent determination of the pattern speed, while the spiral arm pattern speed is substantially lower, with corotation radius near the Sun. The spiral arms are relatively weak in luminosity and one pair may be weaker than the other (Drimmel & Spergel 2001), but the (l, v) -diagram is best reproduced if all four spiral arms have mass.

3.2 Mass of the Bulge and Disk

Scaling the simulated terminal velocity curve of this gas flow model, a rather good fit to the observed HI and CO terminal velocity curve can be obtained for $l \lesssim 50^\circ$ (Englmaier & Gerhard 1999, Bissantz et al. 2003). The model with this scaling, which is equivalent to a maximum disk model in external galaxies, predicts a circular velocity of $v_c = 190 - 200 \text{ km s}^{-1}$ at galactocentric radii 2 - 4 kpc, and a circular velocity at the solar radius $v_c(R_0) \simeq 183 \text{ km s}^{-1}$, $\sim 40 \text{ km s}^{-1}$ lower than the assumed $v_c(R_0) = 220 \text{ km s}^{-1}$. With a similar scaling, a self-consistent N-body model matched to the BG luminosity model (Bissantz, Debattista & Gerhard 2004) also reproduces the radial velocity and proper motion velocity dispersions in several bulge fields. With a reasonable mass function for the bulge and disk stars, this dynamical model in addition accounts for the distribution of microlensing event durations determined by the MACHO collaboration.

In the Milky Way, the degeneracy in such analysis between dark and luminous matter can be lifted – the mass-to-light ratio obtained for the disk and bulge stars from the dynamical fits can be independently verified with microlensing observations. BG give an optical depth map for clump giant stars in their model with maximum M/L. For the clump giant stars the most secure optical depths can be measured; the published values to date are, in units of 10^{-6} , $\tau_{-6} = 2.17^{+0.47}_{-0.38}$

at $(l, b) = (1.5^\circ, -2.68^\circ)$ (MACHO collaboration, Popowski et al. 2005), and $\tau_{-6} = 0.96 \pm 0.3$ at $(l, b) = (2.5^\circ, -4^\circ)$ (EROS collaboration, Afonso et al. 2003). The BG model predicts $\tau_{-6} = 2.4$ and $\tau_{-6} = 1.2$ at these positions, slightly higher but within the errors. More recent EROS data on τ_{-6} at three points in latitude (Hamadache et al. in preparation) also is in good agreement with the BG model. Thus the observed clump giant optical depths now agree quantitatively with the model predictions, for a model in which the inner Galaxy is dominated by baryonic mass. There is no room for dynamically significant dark matter in the inner Galaxy (see also Binney, Bissantz & Gerhard 2000).

3.3 Comparison with Λ CDM and MOND

Milky Way mass models based on disk formation with adiabatic contraction in cuspy dark matter halos in the Λ CDM cosmology were investigated by Klypin et al. (2002). Their favoured model A1 predicts a circular velocity at $R = 2 - 4$ kpc of $\sim 150 \text{ km s}^{-1}$, significantly lower than the $190 - 200 \text{ km s}^{-1}$ predicted by models for the combined NIR, gas dynamical and microlensing data. More consistent with these data is their model B1, which predicts $v_c \sim 185 \text{ km s}^{-1}$ at $R = 2 - 4$ kpc. Model B1 differs from A1 in that a mechanism is assumed by which the disk loses a factor $1.5 - 2$ of its angular momentum to the halo during the collapse. It is also more akin to a maximum disk model and has a larger disk mass than model A1.

Famaey & Binney (2005) have investigated the predictions of the BG model in MOND dynamics. They find that with a suitable but non-standard choice of the MOND interpolating function, the standard acceleration constant a_0 , and a realistic value for the disk M/L, the Galactic terminal curve can be fitted. With the standard interpolating function some dark matter would still be required if $v_c(R_0) = 220 \text{ km s}^{-1}$, but not for $v_c(R_0) = 200 \text{ km s}^{-1}$. However, it may be premature to conclude that MOND can explain the Milky Way dynamics, because of the evidence cited above for a triaxial distribution of spheroid stars (Newberg & Yanny 2005). The SDSS starcounts indicate that the major axis of the spheroid is approximately perpendicular to that of the Galactic bar. The spheroid itself, however, contributes little to the Galactic rotation curve near and outside the solar radius, an elongated disk does not support its elongated orbits, and so the most likely source of triaxial potential would have to be a massive dark halo after all.

4 Origin of the Milky Way Bulge

4.1 Old, α -rich Galactic Bulge Stars and Common Routes to Bulge Formation

The two scenarios commonly discussed for bulge formation are (1) the merging of early disks and fragments, and (2) the secular evolution of disks and bars. The former typically creates large bulges unlike that of the Milky Way, and the latter is likely to create solar abundance, intermediate-age bulges. This is because an extended history of star formation has already enriched the gas before the disk surface density grows large enough to trigger the bar and buckling instabilities.

The Galactic bar does not obviously fit into these scenarios. On the one hand, it is a rapidly rotating bar, so likely descends from the disk. On the other hand, the stars in Baade's window are old, ~ 12 Gyr (e.g., Ortolani et al. 1995), and α -rich (Mc William & Rich 1994, Rich & Oviglia 2005). One possibility is that the inner disk formed rapidly and the bulge bar formed from the disk, all before the iron from SN type IA could significantly enrich the gas. Another is the early formation of an α -rich bulge, followed by the later addition of a barred bulge component from the then \sim solar abundance disk. In this case one expects abundance ratio gradients. In the following, a mechanism is described by which an α -rich bulge component forms from a clump-unstable, star-bursting disk. High-redshift morphological observations suggest that this mechanism may indeed be at work in young late-type disk galaxies, and may thus be of relevance for the origin of the Galactic bulge.

4.2 *Clump Instability in Gas-Rich Disks*

It is well-known that cold gas has a destabilizing influence on galactic disks. Immeli et al. (2004a) studied this in the context of a chemo-dynamical model including a dark halo, stars, and a two-phase interstellar medium with feedback processes from the stars. When most baryons are still in the form of gas, and the cold cloud component from which the stars form can cool (dissipate energy) efficiently, it drives the instability and the galactic disk fragments and forms a number of massive clumps of stars and gas. The clumps spiral to the center of the disk in a few dynamical times and merge there to form a central bulge component in a strong starburst. Noguchi (1998) had earlier described a similar evolution in a collisional particle simulation but, with their model for a star forming 2-phase interstellar medium, Immeli et al. could both verify it in the presence of stellar feedback effects and keep track of stellar metallicities and ages during the evolution. This enabled them to compute luminosities and colours for comparison with photometric observations. Based on these models, Immeli et al. (2004b) argued that several peculiar morphological structures seen in the Hubble Deep Field can be well explained by such a fragmented disk model, including chain and clump cluster galaxies, and they provided predictions for the clump masses, rotation and metallicity properties of these objects as well as for the bulge components that form through this process.

4.3 *Bulge Properties in a Clump Merger Model*

Figure 1 shows a snapshot of the evolution in the clumpy disk phase as well as an edge-on K-band image, the luminosity profile, the metallicity distribution, and the $[\alpha/\text{iron}]$ distribution of bulge stars after completion of the evolution. The figure illustrates the formation of an α -rich bulge component in the early evolution of this disk. For the process to work in this way the galaxy must still be mostly gaseous at the beginning of the evolution; the cold gas must dissipate fairly smoothly into the disk plane, before the main star formation starts; and the clumping and star

formation must start more or less simultaneously throughout a good part of the disk, i.e., the surface density must not be too inhomogeneous. The abundance of chain galaxies and clump cluster galaxies with similar morphologies in the tadpole and ACS deep fields at redshifts around $z \sim 2$ (Elmegreen et al. 2004a,b, Elmegreen & Elmegreen 2005) suggests that many late type and yet bulge-less galaxies may go through such an evolutionary phase. If so, the first parts of the Galactic bulge could well have been formed in a similar way.

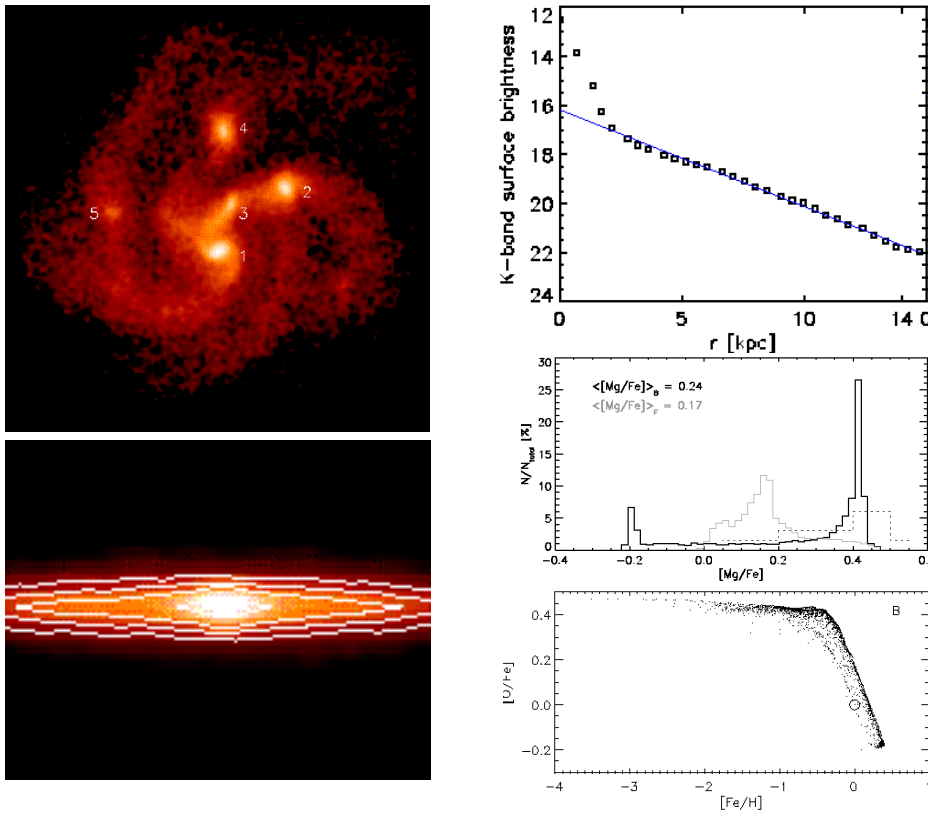


Fig. 1. Left: smoothed stellar surface density of the clumpy disk model of Immeli et al. (2004b) at 1.2 Gyr, with the major clumps numbered (top), and edge-on view in the K band of the inner 11 kpc of model B of Immeli et al. (2004a) at 3.8 Gyr, after the evolution (bottom). Right, from Immeli et al. (2004a): K-band surface brightness profile (top), distribution of $[\text{Mg}/\text{Fe}]$ (middle) and of $[\text{O}/\text{Fe}]$ versus $[\text{Fe}/\text{H}]$ for bulge stars, in model B after 4 Gyr. The middle panel also shows for comparison the metallicity distribution of a secularly evolving model (grey line), and the $[\text{Mg}/\text{Fe}]$ histogram (dotted) of 11 Galactic bulge stars measured by McWilliam & Rich (1994).

References

- Afonso, C., et al., 2003, *A&A*, 404, 145
Babusiaux, C., Gilmore, G., 2005, *MNRAS*, 358, 1309
Battaglia, G., et al., 2005, *astro-ph/0506102*
Binney, J., Bissantz, N., Gerhard, O., 2000, *ApJ*, 537, L99
Binney, J., Gerhard, O., Spergel, D., 1997, *MNRAS*, 288, 365
Bissantz, N., Gerhard, O., 2002, *MNRAS*, 330, 591 (BG)
Bissantz, N., Englmaier, P., Gerhard, O., 2003, *MNRAS*, 340, 949
Bissantz, N., Debattista, V.P., Gerhard, O., 2004, *ApJ*, 601, L155
Dehnen, W., 2000, *AJ*, 119, 800
Drimmel, R., Spergel, D.N., 2001, *ApJ*, 556, 181
Elmegreen, B.G., Elmegreen, D.M., 2005, *ApJ*, 627, 632
Elmegreen, D.M., Elmegreen, B.G., Hirst, A.C., 2004, *ApJ*, 604, L21
Elmegreen, D.M., Elmegreen, B.G., Sheets, C.M., 2004, *ApJ*, 603, 74
Englmaier, P., Gerhard, O., 1999, *MNRAS*, 304, 512
Famaey, B., Binney, J., 2005, 363, 603
Helmi, A., 2004, *ApJ*, 610, L97
Honma, M., Sofue, Y., 1997, *PASJ*, 49, 453
Ibata, R., et al., 2001, *ApJ*, 551, 294
Immeli, A., Samland, M., Gerhard, O., Westera, P., 2004a, *A&A*, 413, 547
Immeli, A., Samland, M., Gerhard, O., Westera, P., 2004b, *ApJ*, 611, 20
Johnston, K.V., Law, D.R., Majewski, S.R., 2005, *ApJ*, 619, 800
Klypin, A., Zhao, H.-S., Somerville, R.S., 2002, *ApJ*, 573, 597
Kochanek, C., 1996, *ApJ*, 457, 228
Little, B., Tremaine, S., 1987, *ApJ*, 320, 493
López-Corredoira, M., et al., 2004, *A&A*, 421, 953
López-Corredoira, M., Cabrera-Lavers, A., Gerhard, O., 2005, *A&A*, 439, 107
Majewski, S.R., et al., 2003, *ApJ*, 599, 1082
Martínez-Delgado, D., et al., 2004, *ApJ*, 601, 242
McWilliam, A., Rich, M.R., 1994, *ApJS*, 91, 749
Newberg, H.J., Yanny, B., 2005, *astro-ph/0502386*
Noguchi, M., 1998, *Nature*, 392, 253
Olling, R.P., Merrifield, M.R., 2000, *MNRAS*, 311, 361
Ortiz, R., Lépine, R.D., 1993, *A&A*, 279, 90
Ortolani, S., et al., 1995, *Nature*, 377, 701
Popowski, P., et al., 2005, *ApJ*, 631, 879
Rich, R.M., Origlia, L., *astro-ph/0506051*
Robin, A.C., et al., 2003, *A&A*, 409, 523
Sakamoto, T., Chiba, M., Beers, T.C., 2003, *A&A*, 397, 899
Stanek, K.Z., et al., 1997, *ApJ*, 477, 163
Wilkinson, M.I., Evans, N.W., 1999, *MNRAS*, 310, 645